Electronic Supplementary Material (ESI) for Inorganic Chemistry Frontiers.

Supporting Information

Architecting 1T-phase material with metal NPs enriching HER kinetics in alkaline and seawater electrolytes

Murugesan Prasanna [a], Hyo Bin Kwak [a], Myung Jun Oh [b], Dong Jin Yoo [a,c*]

[a] Graduate School, Department of Energy Storage/Conversion Engineering (BK21 FOUR), Hydrogen and Fuel Cell Research Center, Jeonbuk National University, 567-Baekje-daero, Deokjin-gu, Jeonju-si, Jeollabuk-do 54896, Republic of Korea.

[b] Department of Carbon Composites Convergence Materials Engineering, Jeonbuk National University, 567 Baekje-daero, Deokjin-gu, Jeonju-si, Jeonbuk-do 54896, Republic of Korea.

[c] Department of Life Science, Jeonbuk National University, 567-Baekje-daero, Deokjin-gu, Jeonju-si, Jeollabuk-do 54896, Republic of Korea.

Corresponding Author E-mail: djyoo@jbnu.ac.kr (Prof. Dong Jin Yoo).

1. Instrumentation for material characterization

The material crystallinity, phase, atomic arrangements, and surface morphology analysis of the prepared electrocatalyst were examined via powder X-ray diffraction (XRD, X'pert-MRD, Pro Philips), 3D imaging Raman spectroscopy with NANO PHOTON, spherical aberration corrected scanning transmission microscopy (CS-TEM) and high-resolution transmission electron microscopy (HR-TEM, JEOL/ JEM-ARM 200F), and field emission scanning electron microscopy (FE-SEM, ZEISS Gemini SEM 500). The metal weight percentage were calculated through inductively coupled plasma- optical emission spectroscopy (ICP-OES) (THERMOF-KR4FB8O iCAP RQ) at the Center for University Wide Research Facilities (CURF) at Jeonbuk National University (JBNU), South Korea. The structural and elemental composition were analyzed via X-ray photoelectron spectroscopy (XPS AxisNova, Kratos, Inc.) at the Korea Basic Science Institute (KBSI) at Jeonbuk National University (JBNU), South Korea.

2. Electrochemical analysis

The electrochemical experiments were performed with conventional three electrode system using Gamry instrument Reference 600 (potentiostat/Galvanostat/ZRA) in seawater and 1 M KOH electrolytes. The electrochemical cell is composed with reference electrode (Ag/AgCl, KCl saturated), counter electrode (graphitic rod), and our designed electrocatalysts in working electrode. Commercial Pt 20 wt.% used for comparison in working electrode. All the materials were coated on Ni-foam (3 mg catalyst in 1×1 cm2) and Fig. S3 shows the location of seawater collection for the analysis. *Operando*-EIS was evaluated from 0.1 Hz to 100kHz with different applied potential, and the observed results were fitted through ZSimpWin software.[1-3] Moreover, the experimental results were measured with help of Ag/AgCl reference electrode, the resulting data was converted to reversible hydrogen electrode (RHE) with the following Nernst equation:

$$E_{RHE} = E_{Ag/AgCl} + 0.059 \times pH + E^{o}_{Ag/AgCl} \quad (1)$$

3. TOF calculation for HER

The hydrogen TOF per site of the Cu@1T-N-W NSs catalyst was derived using the following formula (2):

$$TOF\ per\ site = \frac{Total\ oxygen\ turnovers/cm^2\ \ geometric\ area}{active\ sites/cm^2\ \ geometric\ area} \quad (2)$$

The total number of hydrogen turnovers was calculated according to the formula (3)

$$\#\ H_2 = \left(j\frac{mA}{cm^2}\right)\left(\frac{\frac{1C}{s}}{1000\ mA}\right)\left(\frac{1mol\ e^-}{96485\ C}\right)\left(\frac{1mol\ H_2}{2\ mol\ e^-}\right)\left(\frac{6.022\times10^{23}mol\ H_2}{1mol\ H_2}\right) \quad (3)$$

$$= 3.12\times10^{15}\frac{\frac{H_2}{s}}{cm^2}\ per\ \frac{mA}{cm^2}$$

Then, Cu and W content of the Cu@1T-N-W NSs electrocatalyst was quantified by ICP-OES analysis at about ~37.8 wt.% and 10 wt.%, respectively. Accordingly, the W content of the 1T-N-W NSs electrocatalyst is 65 wt.%. Hence, the active site density based on the Cu and W in Cu@1T-N-W NSs is:

$$\left(\frac{10}{63.5}+\frac{37.8}{183.84}\right)\times\frac{1\ mmol}{100\ mg}\times3\frac{mg}{cm^2}\times6.022\times10^{20}\frac{sites}{1\ mmol} = 6.56\times10^{18}sites\ cm^{-2}$$

Similarly, the 1T-N-W NSs active sites were calculated. Then, the evaluated active sites were substituted in equation (2) to find the TOF of the prepared electrocatalysts.

4. Electrochemically active surface area (ECSA):

The non-faradaic region from the cyclic voltammetry (CV) curve was used to calculate the ECSA value of the developed electrocatalyst with the help of double layer capacitance (C_{dl}) at a scan rate of 10 to 50 mV s^{-1}. The capacitive current was taken from the difference between the anodic current and cathodic current ($\Delta j = j_{anode} - j_{cathode}$). ECSA values are directly proportional to the C_{dl} value (the C_{dl} value is double in the slope calculation) as below:[4]

$$ECSA = \frac{C_{dl}}{C_s} \qquad (4)$$

ECSA = Electrochemical active surface area (ECSA)

C_{dl} = Double layer capacitance

C_s = Specific capacitance (0.040 mF cm^{-2})

5. Tafel slope mechanism

According to the Tafel slope, the alkaline and seawater medium hydrogen evolution reaction (HER) process catalyzed by Cu@1T-N-W NSs material proceeds through Volmer-Heyrovsky mechanism. The HER reaction mechanism can be expressed as:

$$Total\ reaction: 2H_2O + 2e^- \rightarrow H_2 + 2OH^- \qquad (5)$$

$$Volmer\ step: * + H_2O + e^- \rightarrow H^* + OH^- \qquad (6)$$

Heyrovsky step: $H^* + H_2O + e^- \rightarrow H_2 + OH^-$ (7)

6. ECSA normalized LSV:

The current density normalized to the electrochemically active surface area (ECSA) was calculated according to the following equation (8),

$$J_{ECSA} = \frac{I}{S_{ECSA}} \qquad (8)$$

where J_{ECSA} = current density normalized by ECSA,

I = current density (mA),

$S_{ECSA} = C_{dl}/C_s$

7.Faradaic efficiency calculation using Water Displacement Method (WDM):

The Faradic efficiency of Cu@1T-N-W NSs from the overall water splitting was evaluated from the total charge passed through the system at corresponding time intervals using Faraday's law. Here, RuO_2 electrode was used in the anode compartment (for OER).

Using the following equation,

$$V_{Theo} = I * t * V_m / n * F \qquad (9)$$

where

V_{Theo} = Theoretical evolved gas volume,

I = current measured in the experiment (A),

t = measured time (s).

V_m = volumetric molar mass of H_2 in l/mol,

n = number of electrons,

F = Faraday constant = 96485 s A/mol.

Faradaic efficiency (ηF) was determined by ratio of measured gas volume (V_{meas}) and theoretically calculated volumes (V_{Theo}) as given in equation (9),

$$Faradic\ efficiency\ (\eta F) = \frac{V_{meas}}{V_{Theo}}$$

V_{Meas} = Measured evolved gas volume.

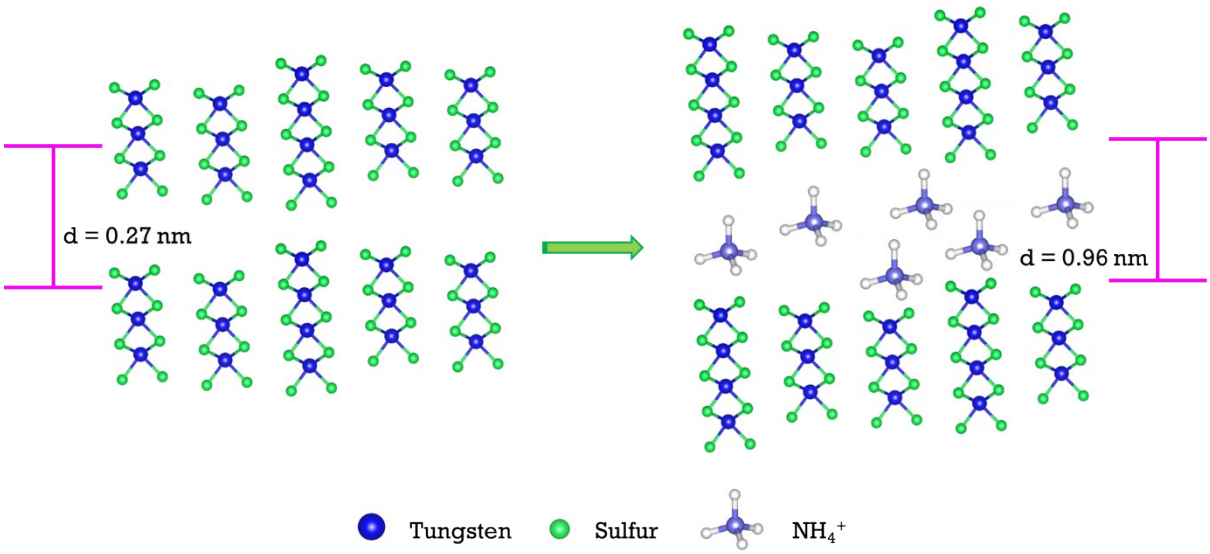

Fig. S1. Schematic representation of ammonium ions intercalation in 1T-N-W NSs.

Initially, the interlayer distance of 1T-WS_2 is 0.27 nm (Fig. S1). This distance was enlarged to 0.96 nm due to the ammonium ions intercalation (NH_4^+), which is higher compared to 2H-WS_2 (0.62 nm).[5] According to Qin Liu, *et al.*,[6] the WS_2 was considered as four types of structural model. This consideration was established by deriving the fundamental calculations on the structural stability and the electrical properties. Here, the hydrogen atoms from NH_4^+ ions directly contact the neighboring sulfur atoms in the WS_2 through hydrogen bonding. As a result, the interlayer distance of the 1T-WS_2 nanosheets were increased with phase stabilization.[6]

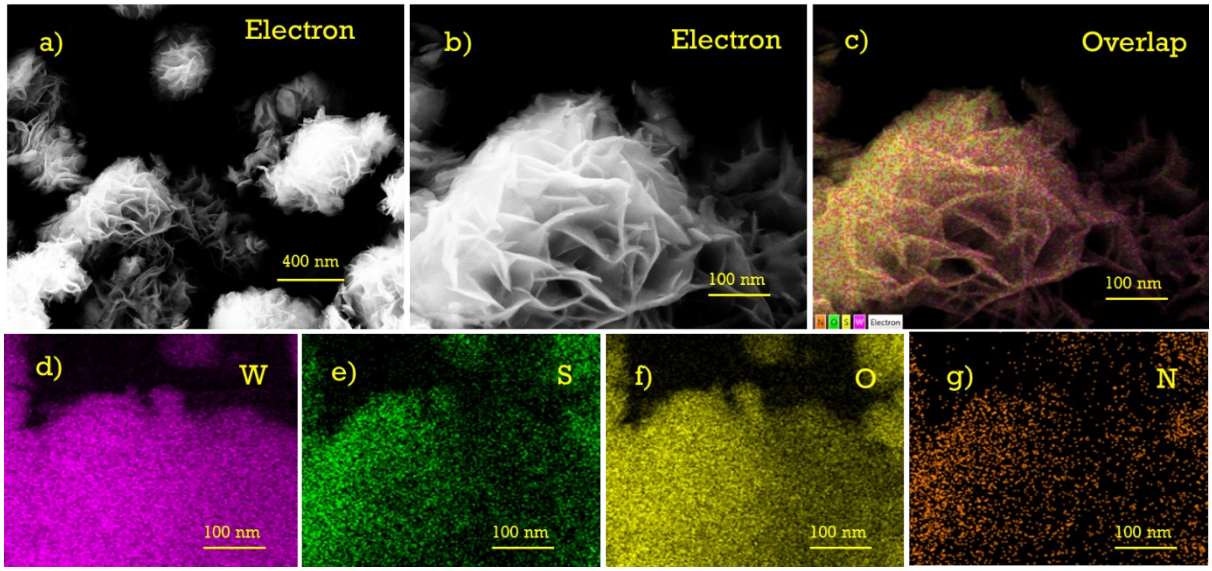

Fig. S2. FE-SEM images of 1T-N-W NSs: (a and b) electron images at different magnifications, (c) EDAX overlapping image, and (d-g) EDAX elemental mapping of W, S, O, and N, respectively.

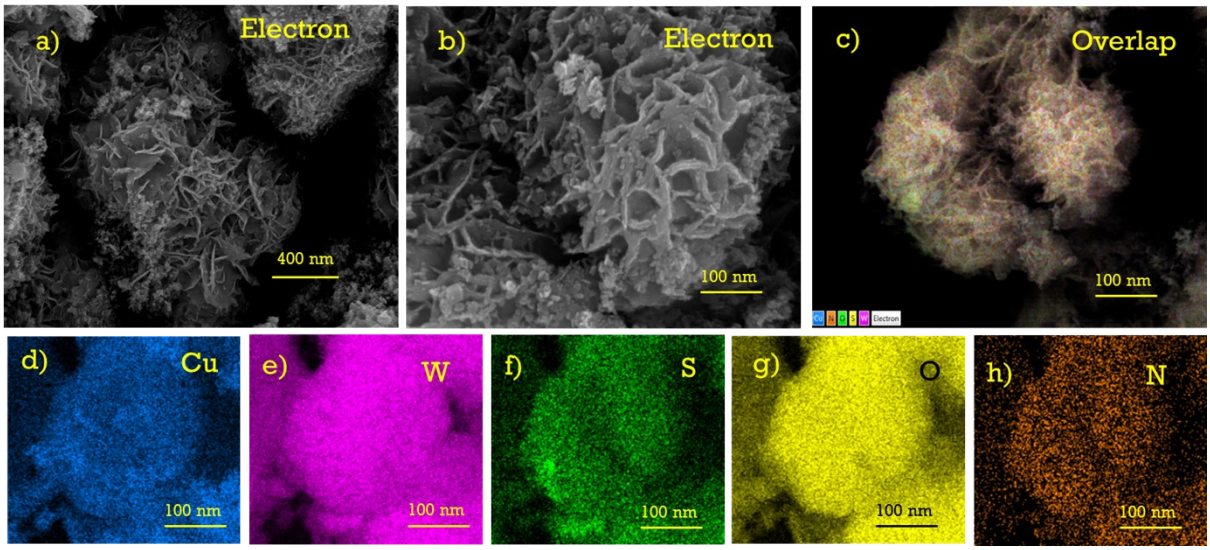

Fig. S3. FE-SEM images of Cu@1T-N-W NSs: (a and b) electron images at different magnifications, (c) EDAX overlapping image, and (d-h) EDAX elemental mapping of Cu, W, S, O, and N, respectively.

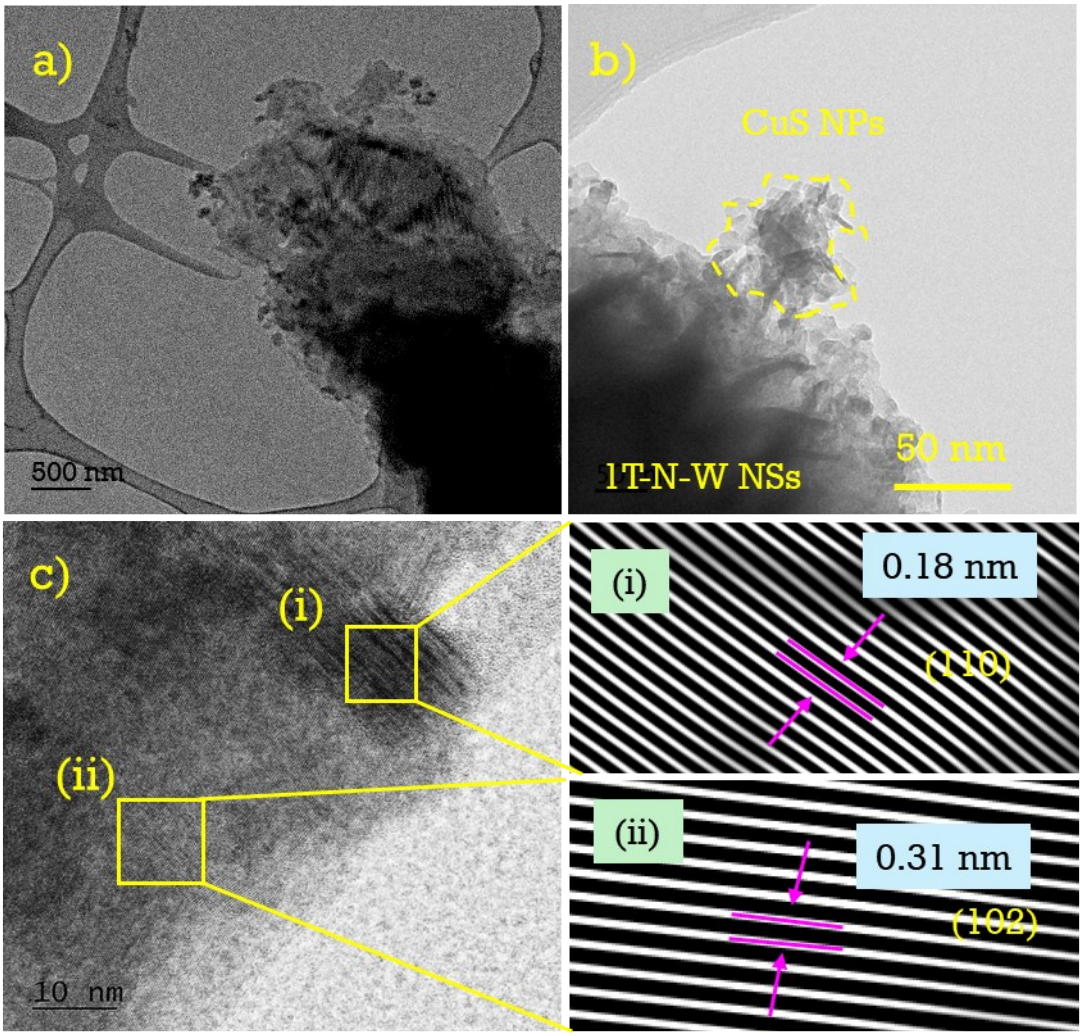

Fig. S4. TEM analysis of Cu@1T-N-W NSs: (a and b) CS-TEM images, (c) HR-TEM analysis.

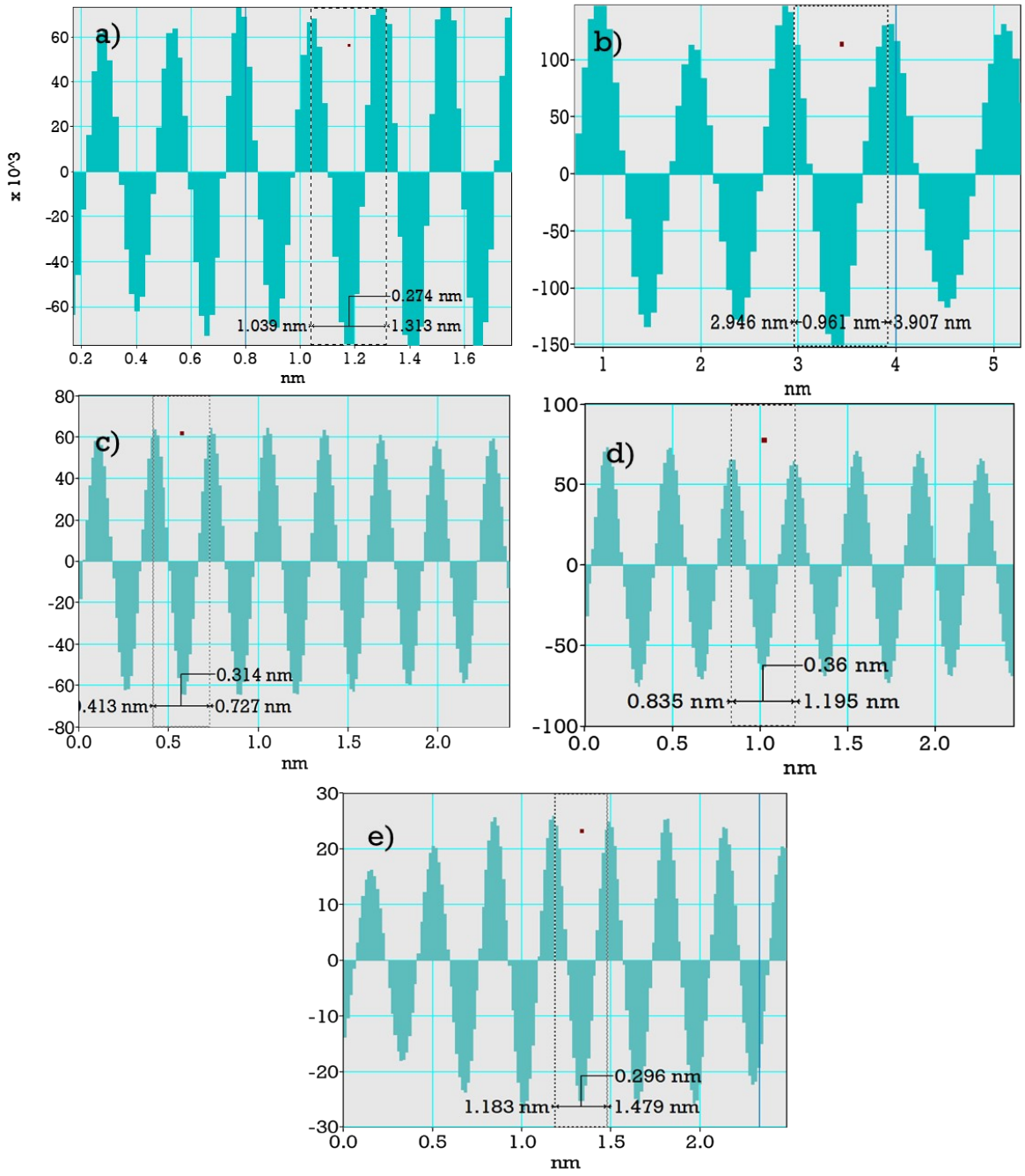

Fig. S5. Evidence of calculated IFFT plane distance for Cu@1T-N-W NSs and 1T-N-W NSs.

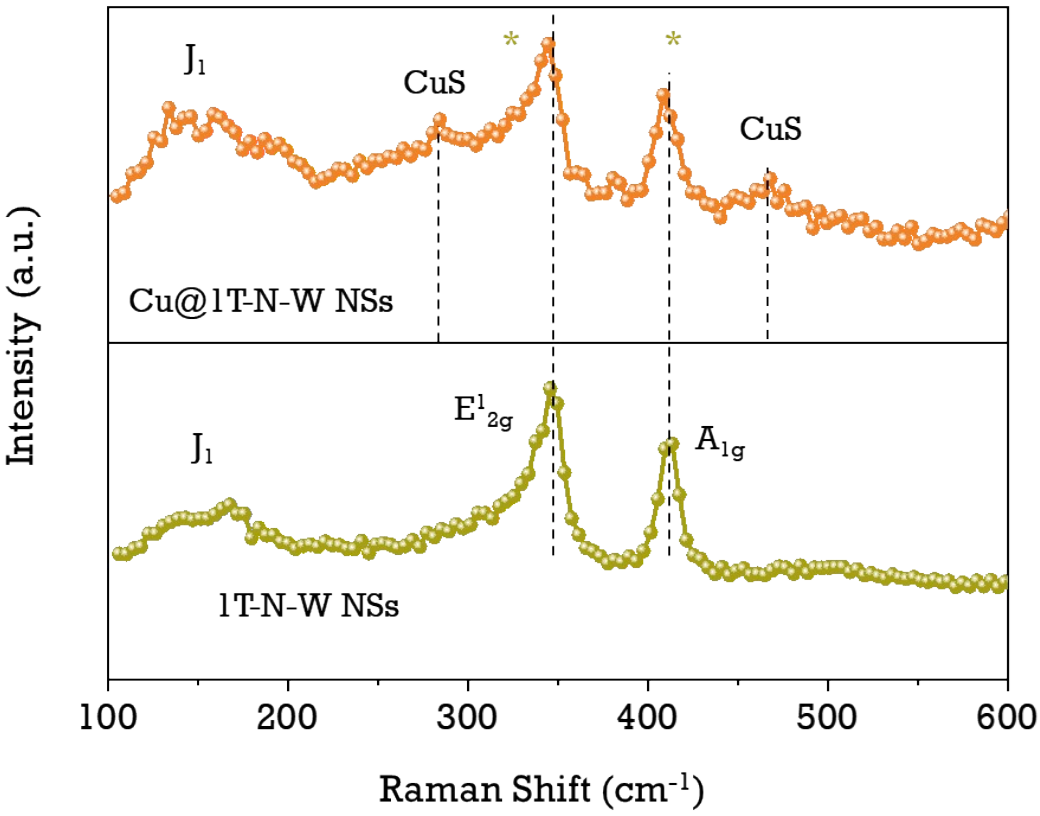

Fig. S6. Raman analysis of Cu@1T-N-W NSs and 1T-N-W NSs.

Fig. S7. Photographic image of the place where seawater water was collected for the experiment (Byeonsan Beach, Republic of Korea).

Table S1: HER overpotential at various current densities in 1 M KOH.

Electrocatalysts	Overpotentials		
	10 mA cm^{-2}	100 mA cm^{-2}	200 mA cm^{-2}
Pt/C 20 wt.%	90.5	151.1	201.8
Cu@1T-N-W NSs	121.8	259.4	336.2
1T-N-W NSs	180.9	363.9	444.5

Table S2: HER overpotential at various current densities in natural seawater + 1 M KOH.

Electrocatalysts	Overpotentials		
	10 mA cm^{-2}	100 mA cm^{-2}	200 mA cm^{-2}
Pt/C 20 wt.%	98.9	200.7	286.6
Cu@1T-N-W NSs	158.2	336.1	434.3
1T-N-W NSs	234.7	402.5	508.1

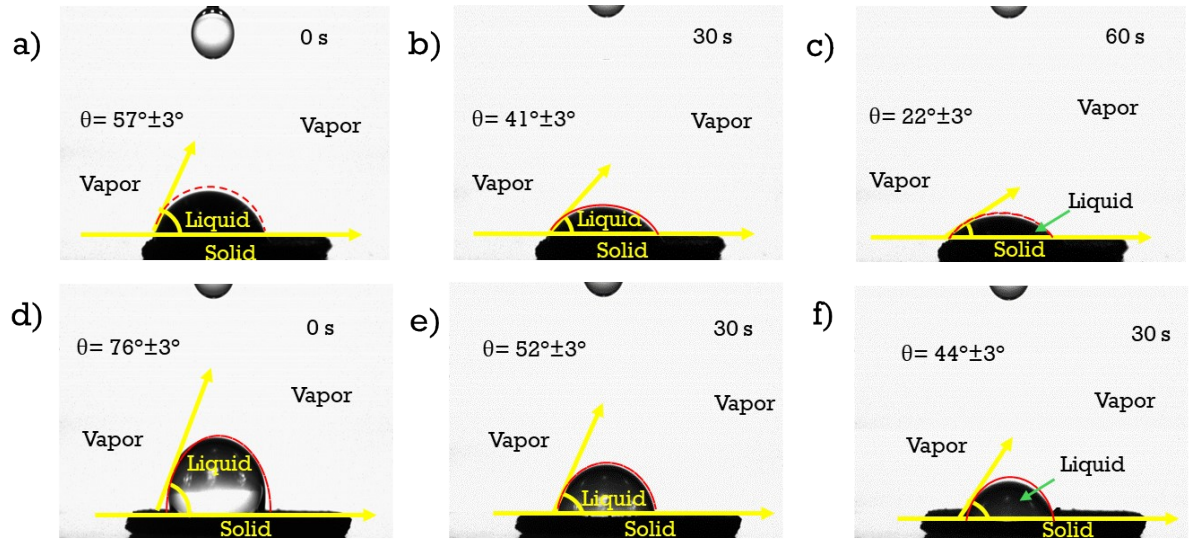

Fig. S8. Contact angle measurements, (a-c) water contact angle measurements of Cu@1T-N-W NSs (d-f) water contact angle measurements of Cu@1T-N-W NSs.

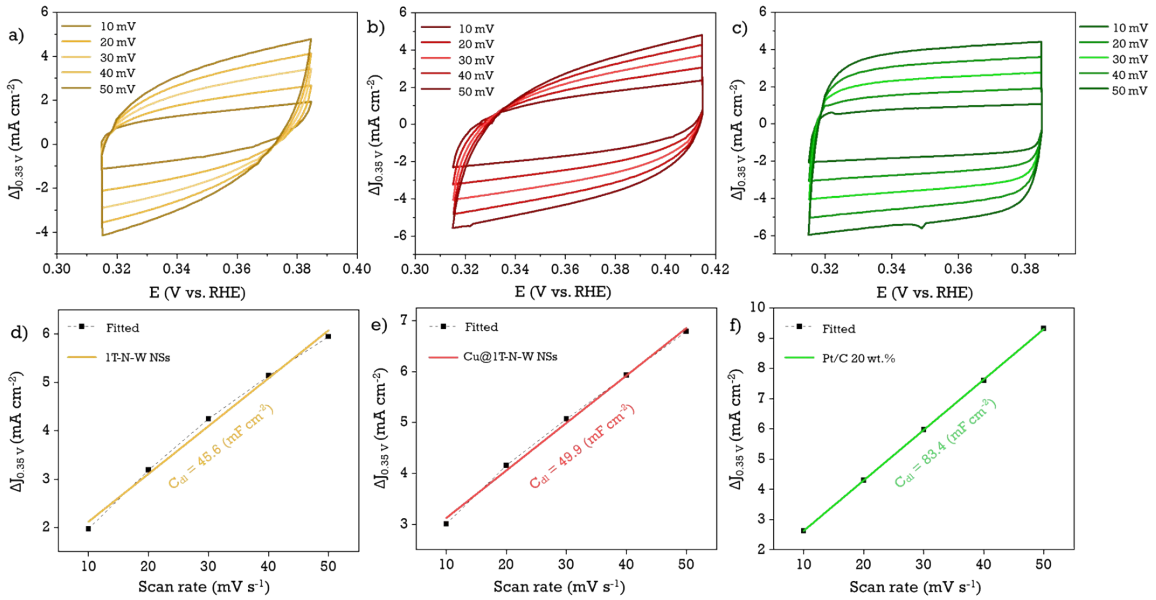

Fig. S9. C_{dl} and ECSA measurements in 1 M KOH solution: (a-c) CV curves at different scan rates (10 to 50 mV s-1) of 1T-N-W NSs, Cu@1T-N-W NSs, and commercial Pt 20 wt.%, respectively. (d-f) respective C_{dl} measurements.

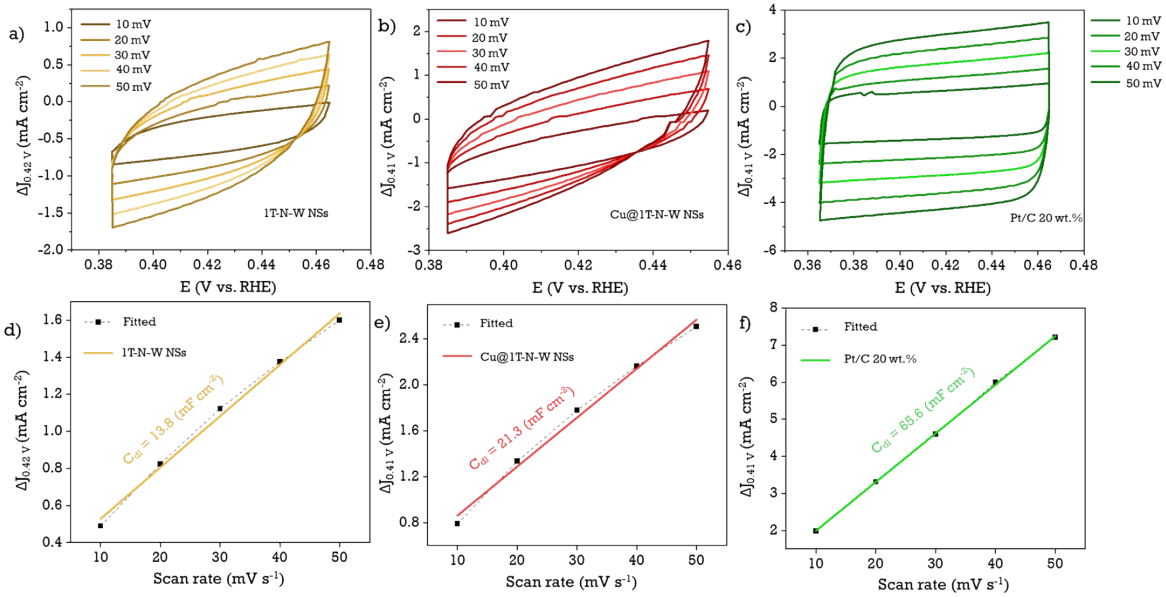

Fig. S10. C_{dl} and ECSA measurements in natural seawater + 1 M KOH: (a-c) CV curves at different scan rates (10 to 50 mV s-1) of 1T-N-W NSs, Cu@1T-N-W NSs, and commercial Pt 20 wt.%, respectively. (d-f) respective C_{dl} measurements.

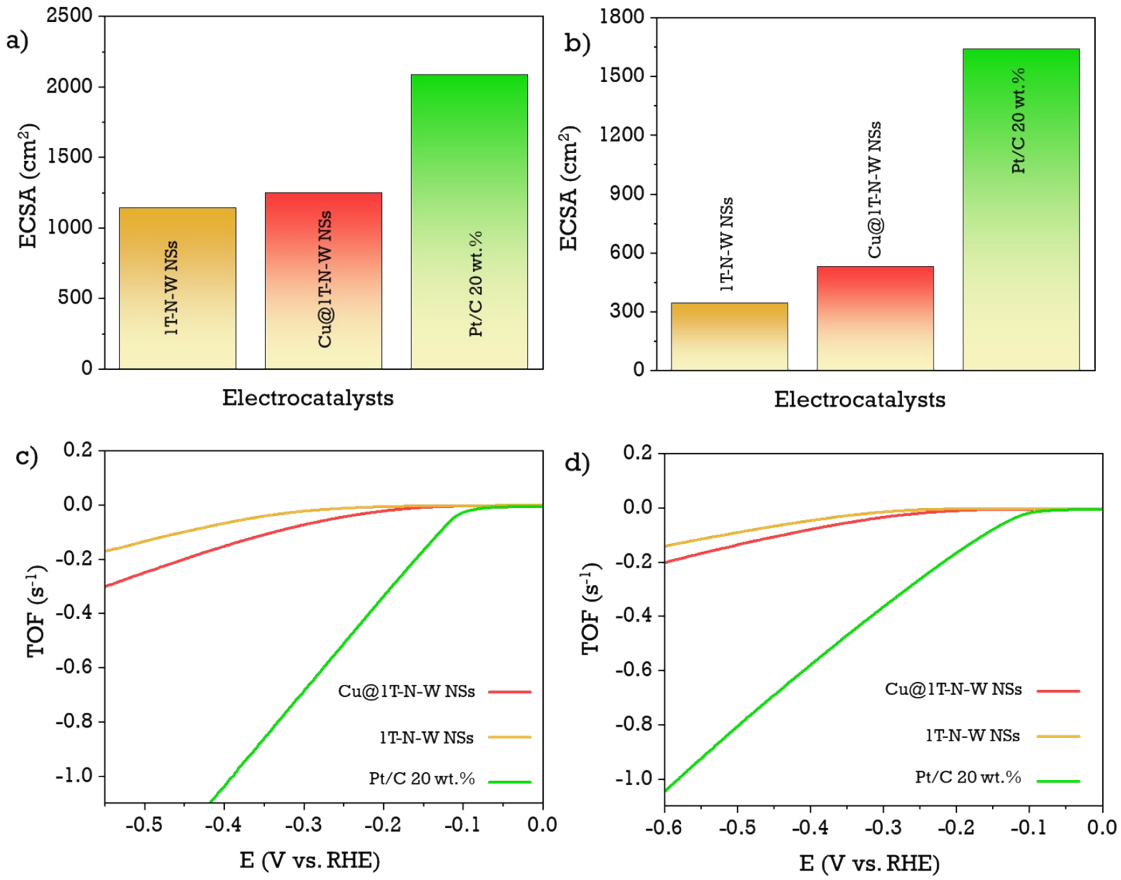

Fig. S11. (a and b) ECSA bar chart in 1 M KOH and natural seawater + 1 M KOH, respectively. (c-d) TOF normalized LSV curves in 1 M KOH and natural seawater + 1 M KOH, respectively.

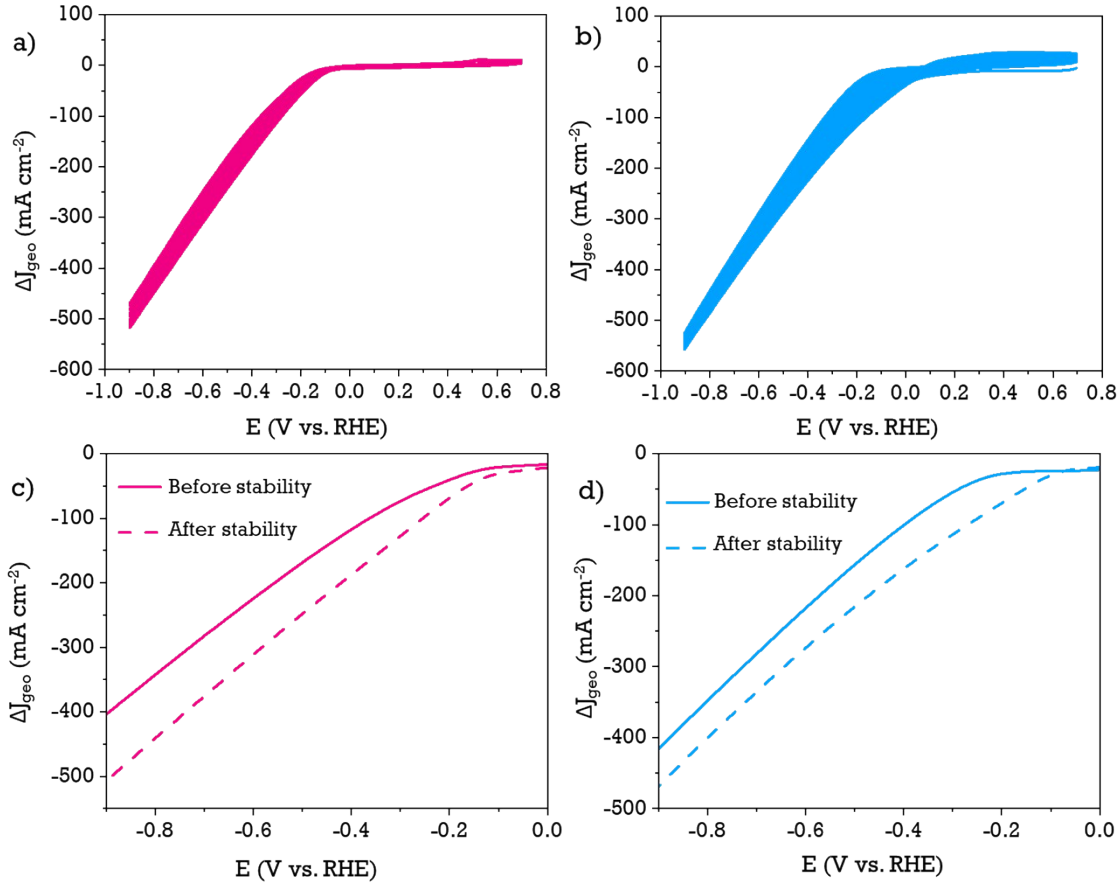

Fig. S12. (a and b) CV stability (1000 cycles) studies of Cu@1T-N-W NS in 1 M KOH and natural seawater + 1 M KOH electrolytes, respectively. (c and d) respective LSV curves of before and after stability.

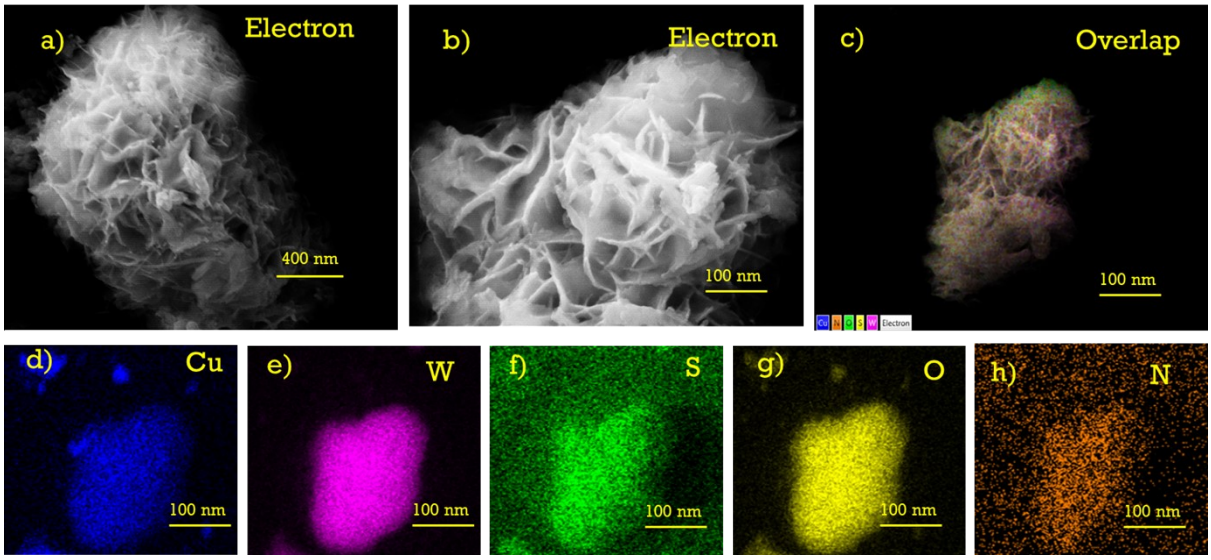

Fig. S13. Post-FE-SEM images of Cu@1T-N-W NSs in natural seawater + 1 M KOH: (a and b) electron images at different magnifications, (c) EDAX overlapping image, and (d-h) EDAX elemental mapping of Cu, W, S, O, and N, respectively.

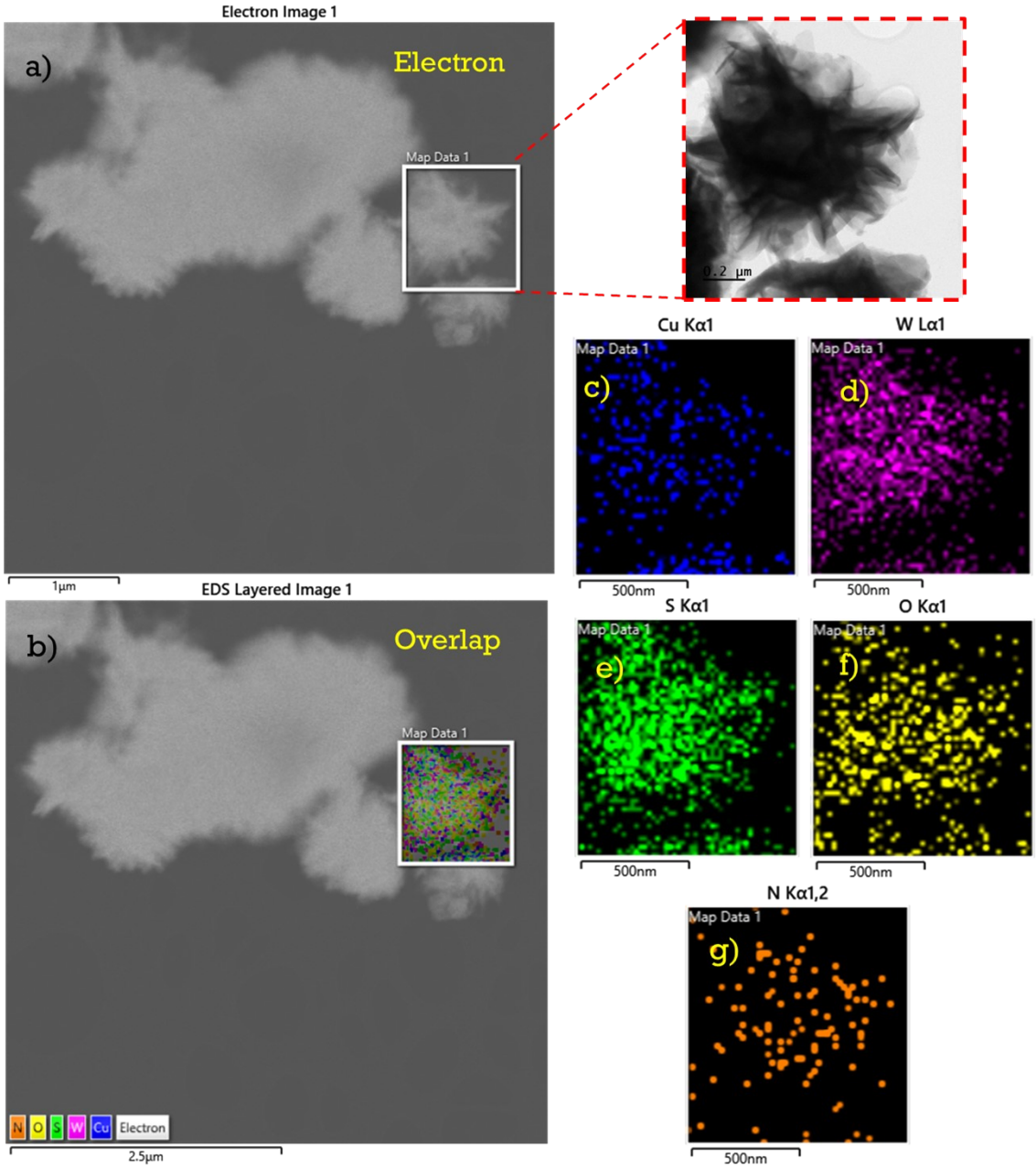

Fig. S14. Post-TEM images of Cu@1T-N-W NSs in natural seawater + 1 M KOH: (a) electron image, (b) HAADF-STEM overlapping image, and (c-g) HAADF-STEM elemental mapping of Cu, W, S, O, and N, respectively.

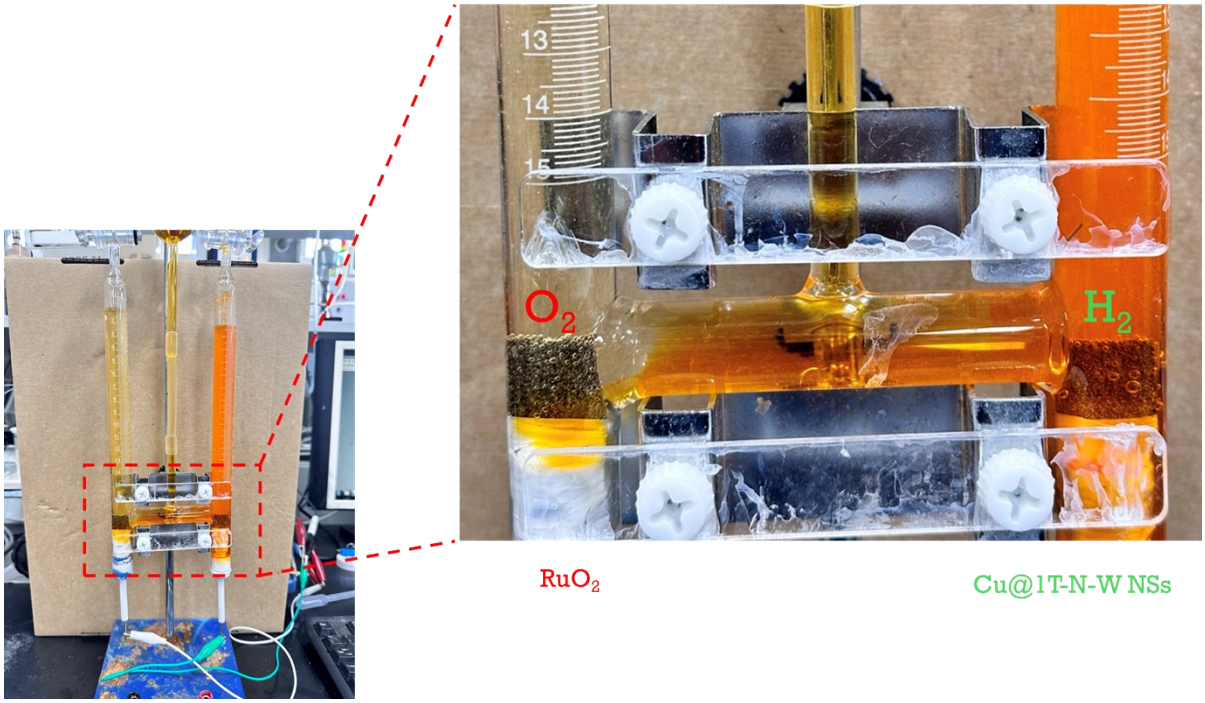

Fig. S15. The real-time picture of FE evaluation

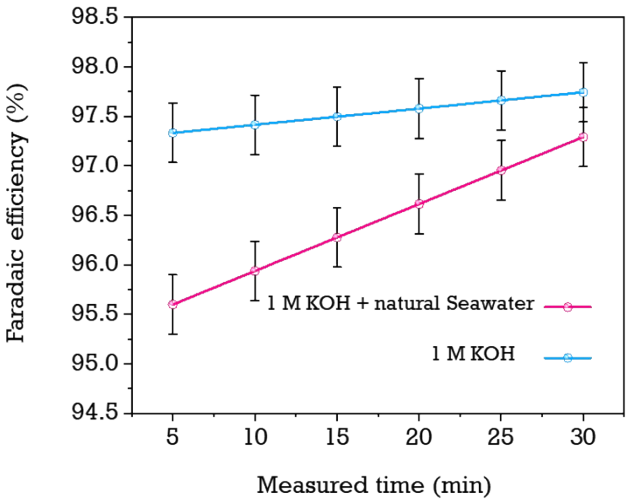

Fig. S16. The derived FE at different time intervals

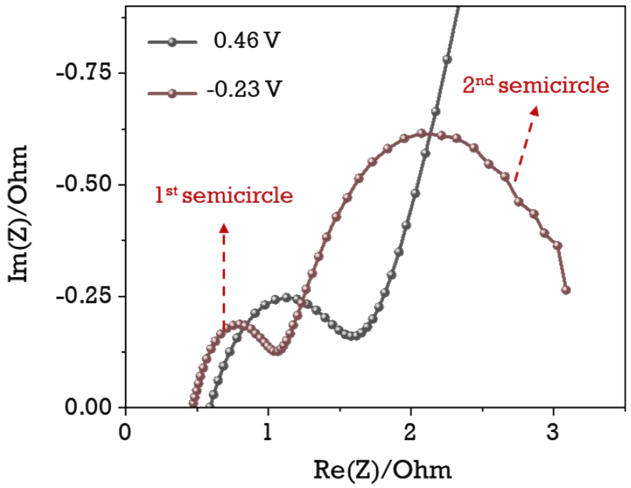

Fig. S17. The Nyquist spectrum of Cu@1T-N-W NSs at different potential (0.46 V is catalyst activation region and -0.23 V is HER region).

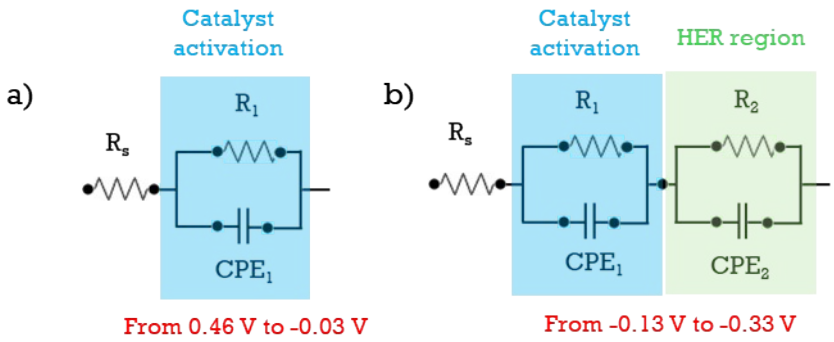

Fig. S18. Equivalent circuit diagram of the electrocatalysts.

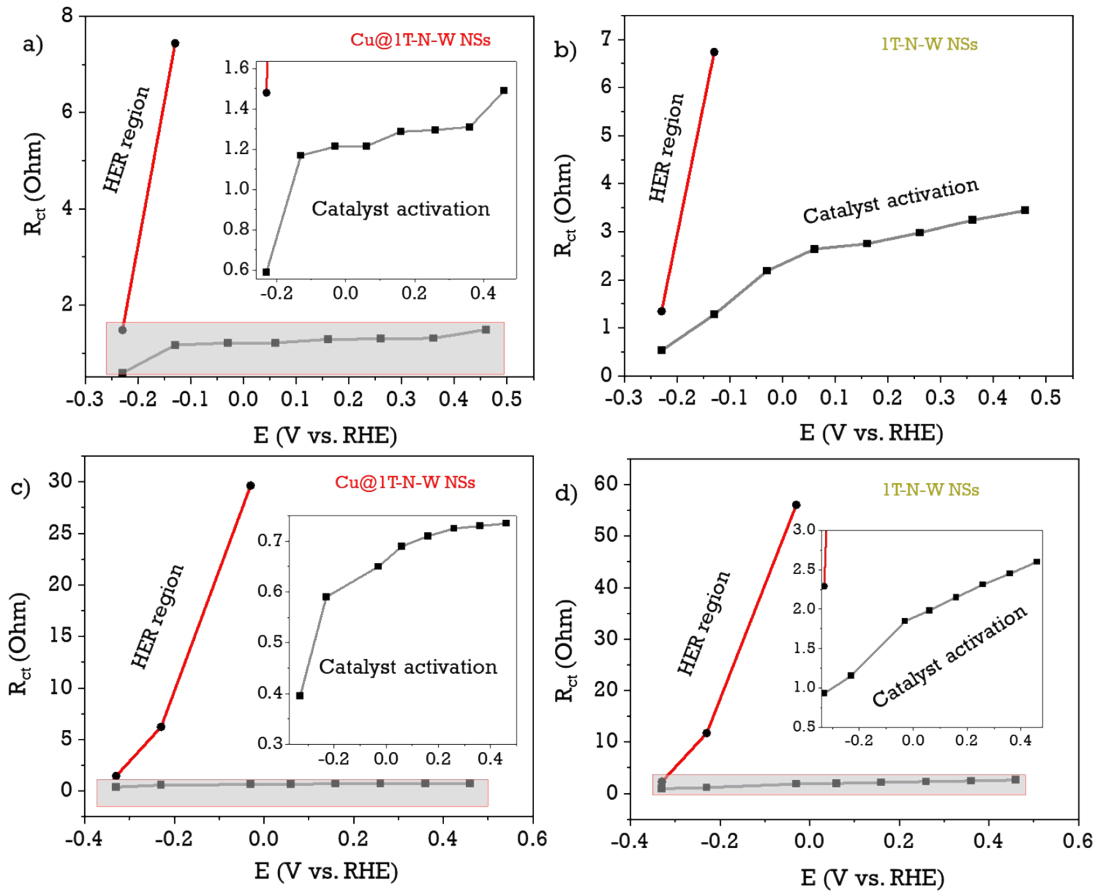

Fig. S19. Fitting of the R_{ct} values of Cu@1T-N-W NSs and 1T-N-W NSs in 1 M KOH and natural seawater + 1 M KOH (in different applied potentials)

Table S3. HER overpotentials and Tafel values of recently reported 1T-WS_2 based electrocatalysts.

Electrocatalysts	Electrolyte	Overpotential @10 mA cm^{-2} (mV)	Tafel values (mV dec^{-1})	Ref.
1T′-D WS2	0.5 M H_2SO_4	200	50.4	7
1T-WS_2	0.5 M H_2SO_4	350@5 mA cm^{-2}	95	8
1T-WS_2	0.5 M H_2SO_4	316	110	9
1T/1T-MWH	0.5 M H_2SO_4	294	99	9
V SACs@1T-WS_2	0.5 M H_2SO_4	185	61	10
1T-WS_2	0.5 M H_2SO_4	118	43	11
1T-CoWS/HMCS	0.5 M H_2SO_4	25	43	12
1T-WS_2NDs	0.5 M H_2SO_4	180	51	13
1T-WS_x_1000 BuLi	0.5 M H_2SO_4	242 ± 7 mV	114 ± 7	14
SLHS-1T-WS_2	0.5 M H_2SO_4	102	46	15
1 T-WS_2|P-5	1 M KOH	190	92.11	16
1 T-WS_2|P-5	0.5 M H_2SO_4	125	73.73	16
1T′-WS_2–$CoCp_2$-14%	0.5 M H_2SO_4	170	40	17
1T′-$Sn_{0.3}W_{0.7}S_2$+CB	0.5 M H_2SO_4	~ 240	81	18
1T-WS_2	0.5 M H_2SO_4	232	63	19
1T-Fe/P-WS_2@CC	1 M KOH	116	65	20
Cu@1T-N-W NSs	**1 M KOH**	**121.8**	**46.3**	**This work**

Table S4. HER overpotentials and Tafel values of recently reported electrocatalysts in 1M KOH.

Electrocatalysts	Electrolyte	Overpotential @10 mA cm^{-2} (mV)	Tafel values (mV dec^{-1})	Ref.
Ni/NiO	1.0 M KOH	226	135	21
Ni-Mo/NG	1.0 M KOH	159	45	22
Ni-Cu	1.0 M KOH	128 mV	57.2 mV/dec^{-1}	23
Co_3O_4–CuO	1.0 M KOH	288	65	24
CoP nanoparticles	1.0 M KOH	87	105	25
NiMoSe/Ti_3C_2Tx@CC	1.0 M KOH	203	45	26
Ni-Ti_3C_2Tx	1.0 M KOH	181.15	56.15	27
$FeCoMnNiSe_2$	1.0 M KOH	142	60.3	28
ZnCoS-1	1.0 M KOH	227	72.39	29
$NiWO_4$-NiO	1.0 M KOH	68	155	30
$Co2P_2O_7$@NC/CF-700	1.0 M KOH	145.7	92.6	31
Ni–Ce–Pr–Ho	1.0 M KOH	78	121.6	32
Co_2P/CoP@NF	1.0 M KOH	61	55.1	33
MoS_2|NiS|MoO_3	1.0 M KOH	91	54.5	34
$NiSe_2$-A	1.0 M KOH	157	76	35
Cu_3P–Ni_2P/NF	1.0 M KOH	103	80	36
Cu@1T-N-W NSs	**1 M KOH**	**121.8**	**46.3**	**This work**

Table S5. HER overpotentials and Tafel values of recently reported electrocatalysts in seawater.

Electrocatalysts	Electrolyte	Overpotential @10 mA cm^{-2} (mV)	Tafel values (mV dec^{-1})	Ref.
Ru/FeTeO	1 M KOH + Seawater	311 @ 3 mA cm^{-2}	61.8	37
(Rh)-WO3	1 M KOH + Seawater	98	84	38
NAU9-500	Artificial seawater	330.2	29.3	39
CoSe/MoSe2	Artificial seawater	164	-	40
CoSe/MoSe2	Alkaline seawater	189	-	40
CoMnTe2-1	1 M KOH + Seawater	136	-	41
Mo3Se4-NiSe	1 M KOH + Seawater	166	90.12	42
$Co_3(PO_4)_2$-MoO_{3-x}/$CoMoO_4$/NF	1 M KOH + Seawater	93	23.69	43
S–Fe(OH)3/NiSe/NF	1 M KOH + Seawater	349@100 mA cm^{-2}	-	44
Ni2P–MoO2	1 M KOH + Seawater	248	-	45
Cu@1T-N-W NSs	**1 M KOH + natural seawater**	**158.2**	**58.5**	**This work**

References

1. Z. Wu, T. Liao, S. Wang, W. Li, B. Wijerathne, W. Hu, A. P. O'Mullane, Y. Gu and Z. Sun, Volcano relationships and a new activity descriptor of 2D transition metal–Fe layered double hydroxides for efficient oxygen evolution reaction, *Materials Horizons*, 2023, **10**, 632-645.
2. B. Ambrose, R. Madhu, K. Ramamurthy, M. Kathiresan and S. Kundu, Viologen-Cucurbit[7]uril Based Polyrotaxanated Covalent Organic Networks: A Metal Free Electrocatalyst for Oxygen Evolution Reaction, *Small*, 2024, **n/a**, 2402403.
3. A. Karmakar, D. Mahendiran, R. Madhu, P. Murugan and S. Kundu, Bypassing the scaling relationship with spin selectivity: construction of Lewis base-functionalized heterostructural 2D nanosheets for enhanced oxygen evolution reaction, *Journal of Materials Chemistry A*, 2023, **11**, 16349-16362.
4. S. Ramakrishnan, D. B. Velusamy, S. Sengodan, G. Nagaraju, D. H. Kim, A. R. Kim and D. J. Yoo, Rational design of multifunctional electrocatalyst: An approach towards efficient overall water splitting and rechargeable flexible solid-state zinc–air battery, *Applied Catalysis B: Environmental*, 2022, **300**.
5. M. Prasanna, N. Logeshwaran, S. Ramakrishnan and D. J. Yoo, Metallic 1T-N-WS2/WO3 Heterojunctions Featuring Interface-Engineered Cu–S Configuration for Selective Electrochemical CO2 Reduction Reaction, *Small*, 2024, **20**, 2306165.
6. Q. Liu, X. Li, Z. Xiao, Y. Zhou, H. Chen, A. Khalil, T. Xiang, J. Xu, W. Chu, X. Wu, J. Yang, C. Wang, Y. Xiong, C. Jin, P. M. Ajayan and L. Song, Stable Metallic 1T-WS2 Nanoribbons Intercalated with Ammonia Ions: The Correlation between Structure and Electrical/Optical Properties, *Advanced Materials*, 2015, **27**, 4837-4844.
7. Z. Liu, N. Li, C. Su, H. Zhao, L. Xu, Z. Yin, J. Li and Y. Du, Colloidal synthesis of 1T' phase dominated WS2 towards endurable electrocatalysis, *Nano Energy*, 2018, **50**, 176-181.
8. H. U. Kim, V. Kanade, M. Kim, K. S. Kim, B. S. An, H. Seok, H. Yoo, L. E. Chaney, S. I. Kim, C. W. Yang, G. Y. Yeom, D. Whang, J. H. Lee and T. Kim, Wafer-Scale and Low-Temperature Growth of 1T-WS2 Film for Efficient and Stable Hydrogen Evolution Reaction, *Small*, 2020, **16**, e1905000.
9. H. Seok, M. Kim, J. Cho, E. Kim, S. Son, K.-W. Kim, J. K. Kim, P. J. Yoo, M. Kim, H.-U. Kim and T. Kim, Tailoring Polymorphic Heterostructures of MoS2–WS2 (1T/1T, 2H/2H) for Efficient Hydrogen Evolution Reaction, *ACS Sustainable Chemistry & Engineering*, 2023, **11**, 568-577.
10. A. Han, X. Zhou, X. Wang, S. Liu, Q. Xiong, Q. Zhang, L. Gu, Z. Zhuang, W. Zhang, F. Li, D. Wang, L. J. Li and Y. Li, One-step synthesis of single-site vanadium substitution in 1T-WS2 monolayers for enhanced hydrogen evolution catalysis, *Nat Commun*, 2021, **12**, 709.
11. Q. He, L. Wang, K. Yin and S. Luo, Vertically Aligned Ultrathin 1T-WS(2) Nanosheets Enhanced the Electrocatalytic Hydrogen Evolution, *Nanoscale Res Lett*, 2018, **13**, 167.
12. C. Yue, F. Sun, N. Liu, Y. Liu, W. Bao, X. Zhang, C. Zhang, S. Ma, Y. Zhou, C. Feng and Y. Lu, High phase purity of stable 1T-phase Co-doped WS2 for full pH hydrogen evolution reaction in water and seawater, *Fuel*, 2024, **357**, 129668.
13. X. Zhao, X. Ma, J. Sun, D. Li and X. Yang, Enhanced Catalytic Activities of Surfactant-Assisted Exfoliated WS2 Nanodots for Hydrogen Evolution, *ACS Nano*, 2016, **10**, 2159-2166.

14. M. P. Browne, F. Novotný, C. L. Manzanares Palenzuela, J. Šturala, Z. Sofer and M. Pumera, 2H and 2H/1T-Transition Metal Dichalcogenide Films Prepared via Powderless Gas Deposition for the Hydrogen Evolution Reaction, *ACS Sustainable Chemistry & Engineering*, 2019, **7**, 16440-16449.
15. B. Li, K. Nie, Y. Zhang, L. Yi, Y. Yuan, S. Chong, Z. Liu and W. Huang, Engineering Single-Layer Hollow Structure of Transition Metal Dichalcogenides with High 1T-Phase Purity for Hydrogen Evolution Reaction, *Advanced Materials*, 2023, **35**, 2303285.
16. L. Sun, M. Gao, Z. Jing, Z. Cheng, D. Zheng, H. Xu, Q. Zhou and J. Lin, 1 T-Phase Enriched P doped WS2 nanosphere for highly efficient electrochemical hydrogen evolution reaction, *Chemical Engineering Journal*, 2022, **429**, 132187.
17. I. H. Kwak, H. G. Abbas, I. S. Kwon, Y. C. Park, J. Seo, M. K. Cho, J.-P. Ahn, H. W. Seo, J. Park and H. S. Kang, Intercalation of cobaltocene into WS2 nanosheets for enhanced catalytic hydrogen evolution reaction, *Journal of Materials Chemistry A*, 2019, **7**, 8101-8106.
18. G. Shao, X.-X. Xue, B. Wu, Y.-C. Lin, M. Ouzounian, T. S. Hu, Y. Xu, X. Liu, S. Li, K. Suenaga, Y. Feng and S. Liu, Template-Assisted Synthesis of Metallic 1T′-Sn0.3W0.7S2 Nanosheets for Hydrogen Evolution Reaction, *Advanced Functional Materials*, 2020, **30**, 1906069.
19. C. Tan, Z. Luo, A. Chaturvedi, Y. Cai, Y. Du, Y. Gong, Y. Huang, Z. Lai, X. Zhang, L. Zheng, X. Qi, M. H. Goh, J. Wang, S. Han, X.-J. Wu, L. Gu, C. Kloc and H. Zhang, Preparation of High-Percentage 1T-Phase Transition Metal Dichalcogenide Nanodots for Electrochemical Hydrogen Evolution, *Advanced Materials*, 2018, **30**, 1705509.
20. D. R. Paudel, U. N. Pan, T. I. Singh, C. C. Gudal, N. H. Kim and J. H. Lee, Fe and P Doped 1T-Phase Enriched WS23D-Dendritic Nanostructures for Efficient Overall Water Splitting, *Applied Catalysis B: Environmental*, 2021, **286**, 119897.
21. A. Y. Faid, A. O. Barnett, F. Seland and S. Sunde, Ni/NiO nanosheets for alkaline hydrogen evolution reaction: In situ electrochemical-Raman study, *Electrochimica Acta*, 2020, **361**, 137040.
22. S. Xue, W. Zhang, Q. Zhang, J. Du, H.-M. Cheng and W. Ren, Heterostructured Ni–Mo–N nanoparticles decorated on reduced graphene oxide as efficient and robust electrocatalyst for hydrogen evolution reaction, *Carbon*, 2020, **165**, 122-128.
23. M. Y. Gao, C. Yang, Q. B. Zhang, Y. W. Yu, Y. X. Hua, Y. Li and P. Dong, Electrochemical fabrication of porous Ni-Cu alloy nanosheets with high catalytic activity for hydrogen evolution, *Electrochimica Acta*, 2016, **215**, 609-616.
24. A. Tahira, Z. H. Ibupoto, M. Willander and O. Nur, Advanced Co3O4–CuO nano-composite based electrocatalyst for efficient hydrogen evolution reaction in alkaline media, *International Journal of Hydrogen Energy*, 2019, **44**, 26148-26157.
25. S. Luo, P. Hei, R. Wang, J. Yin, W. Hong, S. Liu, Z. Bai and T. Jiao, Facile synthesis of cobalt phosphide nanoparticles as highly active electrocatalysts for hydrogen evolution reaction, *Colloids and Surfaces A: Physicochemical and Engineering Aspects*, 2020, **600**, 124925.
26. M. Saquib, N. Srivastava, P. Arora and A. C. Bhosale, NiMoSe/Ti3C2Tx MXene @ CC as a highly operative bifunctional electrocatalyst for hydrogen and oxygen evolution reactions in an alkaline medium, *International Journal of Hydrogen Energy*, 2024, **59**, 1132-1142.
27. K. Gothandapani, G. Tamil Selvi, R. Sofia Jennifer, V. Velmurugan, S. Pandiaraj, M. Muthuramamoorthy, S. Pitchaimuthu, V. Raghavan, A. C. Josephine Malathi, A. Alodhayb and A. Nirmala Grace, Ni-Ti3C2 MXene composite derived from Ni-metal

organic framework for electrochemical hydrogen evolution reaction in acidic and alkaline medium, *International Journal of Hydrogen Energy*, 2024, **52**, 1164-1171.
28. Z. Liu, X. Guo, T. Cui, S. Mu, Z. Ni, C. Zhang and S. Lu, Porous freestanding FeCoMnNiSe2 medium-entropy bifunctional electrocatalyst for oxygen and hydrogen evolution reactions in alkaline medium, *Journal of Power Sources*, 2024, **592**, 233956.
29. A. Prabhakaran Shyma and R. Sellappan, Synergistic performance of Zn2+ incorporated bimetallic Cobalt sulfide for the hydrogen evolution reaction in an alkaline medium, *Journal of Physics and Chemistry of Solids*, 2023, **178**, 111332.
30. A. Gaur, Krishankant, V. Pundir, T. Maruyama, C. Bera and V. Bagchi, Electronic redistribution over the active sites of NiWO4-NiO induces collegial enhancement in hydrogen evolution reaction in alkaline medium, *Journal of Colloid and Interface Science*, 2023, **641**, 82-90.
31. Y. Han, J. Lin, H. Zhou, L. Guo and Y. Wang, Self-standing Co2P2O7@N-doped carbon/carbon foams for hydrogen evolution reaction in alkaline medium, *Diamond and Related Materials*, 2023, **135**, 109843.
32. W. Liu, W. Tan, H. He, Y. Peng, Y. Chen and Y. Yang, One–step electrodeposition of Ni–Ce–Pr–Ho/NF as an efficient electrocatalyst for hydrogen evolution reaction in alkaline medium, *Energy*, 2022, **250**, 123831.
33. G. Huang, W. Liang, Y. Wu, J. Li, Y. Q. Jin, H. Zeng, H. Zhang, F. Xie, J. Chen, N. Wang, Y. Jin and H. Meng, Co2P/CoP hybrid as a reversible electrocatalyst for hydrogen oxidation/evolution reactions in alkaline medium, *Journal of Catalysis*, 2020, **390**, 23-29.
34. C. Wang, B. Tian, M. Wu and J. Wang, Revelation of the Excellent Intrinsic Activity of MoS2|NiS|MoO3 Nanowires for Hydrogen Evolution Reaction in Alkaline Medium, *ACS Applied Materials & Interfaces*, 2017, **9**, 7084-7090.
35. L. Zhai, T. W. Benedict Lo, Z.-L. Xu, J. Potter, J. Mo, X. Guo, C. C. Tang, S. C. Edman Tsang and S. P. Lau, In Situ Phase Transformation on Nickel-Based Selenides for Enhanced Hydrogen Evolution Reaction in Alkaline Medium, *ACS Energy Letters*, 2020, **5**, 2483-2491.
36. X. Jin, J. Li, Y. Cui, X. Liu, X. Zhang, J. Yao and B. Liu, Cu3P–Ni2P Hybrid Hexagonal Nanosheet Arrays for Efficient Hydrogen Evolution Reaction in Alkaline Solution, *Inorganic Chemistry*, 2019, **58**, 11630-11635.
37. K. Li, X. Liu, X. Wang, S. Wu, W. Li, J. Chi and L. Wang, Iron-based heterojunction activate strong metal-support interaction enabling hydrogen evolution reaction at ampere-level current density in seawater, *Nano Energy*, 2024, **123**, 109417.
38. N.-A. Nguyen, E. Chuluunbat, T. A. Nguyen and H.-S. Choi, High electrocatalytic activity of Rh-WO3 electrocatalyst for hydrogen evolution reaction under the acidic, alkaline, and alkaline-seawater electrolytes, *International Journal of Hydrogen Energy*, 2023, **48**, 32686-32698.
39. Z. Ren, S. Wang, J. Yu, F. Mao, K. Wang and H. Wu, Cu/MoO2 Schottky heterojunction derived from a new designed POMOFs in-situ as high efficient electrocatalysts for hydrogen evolution reaction in universal-pH electrolytes and seawater, *Chemical Engineering Journal*, 2023, **470**, 144107.
40. J. Sun, J. Li, Z. Li, C. Li, G. Ren, Z. Zhang and X. Meng, Modulating the Electronic Structure on Cobalt Sites by Compatible Heterojunction Fabrication for Greatly Improved Overall Water/Seawater Electrolysis, *ACS Sustainable Chemistry & Engineering*, 2022, **10**, 9980-9990.
41. S. C. Karthikeyan, S. Prabhakaran, R. S. Kumar, S. Ramakrishnan, A. R. Kim, D. H. Kim and D. J. Yoo, High-efficiency sustainable energy driven alkaline/seawater

electrolysis using a novel hetero-structured non-noble bimetal telluride nanorods, *Materials Today Nano*, 2023, **24**, 100412.
42. M. B. Poudel, N. Logeshwaran, S. Prabhakaran, A. R. Kim, D. H. Kim and D. J. Yoo, Low-Cost Hydrogen Production from Alkaline/Seawater over a Single-Step Synthesis of Mo3Se4-NiSe Core–Shell Nanowire Arrays, *Advanced Materials*, 2024, **36**, 2305813.
43. M. Yang, B. Shi, Y. Tang, H. Lu, G. Wang, S. Zhang, M. T. Sarwar, A. Tang, L. Fu, M. Wu and H. Yang, Interfacial Chemical Bond Modulation of Co3(PO4)2-MoO3–x Heterostructures for Alkaline Water/Seawater Splitting, *Inorganic Chemistry*, 2023, **62**, 2838-2847.
44. C. Yang, X. Jiang, Y. Li, J. Zeng and H.-P. Liang, Construction of S-modified Amorphous Fe(OH)3 on NiSe Nanowires as Bifunctional Electrocatalysts for Efficient Seawater Splitting, *ACS Applied Nano Materials*, 2024, **7**, 3960-3967.
45. L. P. Phan, T. T. N. Tran, T.-K. Truong, J. Yu, H.-V. T. Nguyen, T. B. Phan, N. H. Thi Tran and N. Q. Tran, Highly Efficient and Stable Hydrogen Evolution from Natural Seawater by Boron-Doped Three-Dimensional Ni2P–MoO2 Heterostructure Microrod Arrays, *The Journal of Physical Chemistry Letters*, 2023, **14**, 7264-7273.